LANGMUIR Article
Cite This: Langmuir 2019, 35, 6708−6718
pubs.acs.org/Langmuir

Close-Packed Langmuir Monolayers of Saccharide-Based Carbon Dots at the Air−Subphase Interface

Elif S. Seven,[†] Shiv K. Sharma,[†] Dihya Meziane,[†] Yiqun Zhou,[†] Keenan J. Mintz,[†] Raja R. Pandey,[‡] Charles C. Chusuei,[‡] and Roger M. Leblanc*[,†]

[†]Department of Chemistry, University of Miami, 1301 Memorial Drive, Coral Gables, Florida 33146, United States
[‡]Department of Chemistry, Middle Tennessee State University, 440 Friendship Street, Murfreesboro, Tennessee 37132, United States

Supporting Information

ABSTRACT: Carbon dots (CDs) are zero-dimensional carbon-based spherical nanoparticles with diameters less than 10 nm. Here, we report for the first time CDs forming stable Langmuir monolayers at the air−subphase interface. Langmuir monolayers are of great interest both fundamentally to study the interactions at the interfaces and for many applications such as the development of sensors. However, CDs usually do not form Langmuir monolayers because of their highly hydrophilic nature. In this study, amphiphilic CDs were prepared through hydrothermal carbonization using saccharides as the precursors. The surface chemistry behavior and optical properties of CDs at the air−subphase interface were studied. CDs derived from saccharides consistently formed stable Langmuir monolayers which show all essential phases, namely, gas, liquid-expanded, liquid-condensed, and solid phases. The compression−decompression cycle method showed minimum hysteresis (4.3%), confirming the retaining capacity of the CDs as a monolayer. Limiting CD areas from surface pressure−area isotherm at the air−subphase interface were used to calculate the average diameter of the CDs at the air−subphase interface. UV/vis absorption spectra of CDs dispersed in water and in Langmuir monolayers had the same bands in the UV region. The intensity of the UV/vis absorption increases with increasing surface pressure at the air−subphase interface. Interestingly, photoluminescence (PL) of the Langmuir monolayer of CDs was excitation-independent, whereas the same CDs had excitation-dependent PL when dispersed in water.

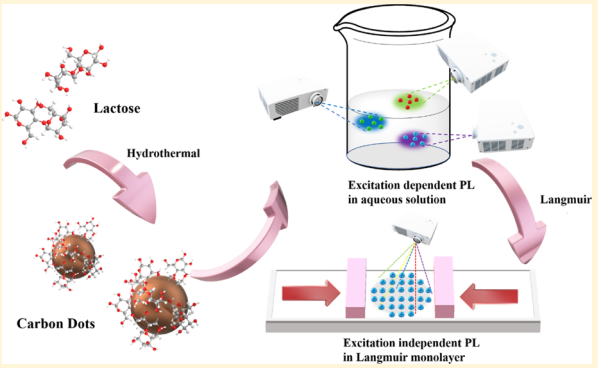

INTRODUCTION

Carbon dots (CDs) are a new type of zero-dimensional carbon-based nanomaterials discovered in 2004 during the synthesis of carbon nanotubes.[1] Since their discovery, CDs have attracted tremendous attention because of their unique photoluminescent (PL) properties, small size (<10 nm), nontoxicity, biocompatibility, and various surface functionalities.[2−8] Several research groups used CDs for in vitro and in vivo bioimaging. However, the PL origin of CDs is still a subject of scientific debate. Langmuir monolayer methodology is one of the techniques that can offer insights for the origin of PL of CDs.[9] However, none of the CDs synthesized until now, per our knowledge, have been reported as forming Langmuir monolayers. Here, we report for the first time, CDs forming stable Langmuir monolayers at the air−subphase interface. We prepared and characterized CDs in bulk solution and solid powder, and then analyzed both the surface and spectroscopic properties of the Langmuir monolayer of CDs. The results contribute to the origin of the CDs' PL emission debate with a unique point of view.

The surface properties and the entailing potential applications of CDs vary widely depending on the precursor molecules and preparation methods. As an interesting example, CDs have high affinity for the receptors of their precursor molecules in biological systems, which makes them excellent candidates for targeted drug delivery systems.[10,11] In this study, we used a simple, straightforward, and green preparation method to prepare luminescent CDs that can form stable Langmuir monolayers. It is unexpected for the CDs to form Langmuir monolayers because of their small size, highly hydrophilic surface groups and hence the great water dispersity. For example, graphene oxide nanosheets with considerably larger size do not form stable monolayers. This requires particles of large size, special methods of deposition, and certain additives in the aqueous subphase and in the monolayer-forming aqueous solution. Different from typical CDs, in addition to water, the saccharide-based CDs also have a certain dispersibility in organic solvents such as methanol and acetone, which has been confirmed by fluorescence measurements. Dispersibility in both water and organic solvents

Received: March 28, 2019
Revised: April 19, 2019
Published: April 30, 2019

DOI: 10.1021/acs.langmuir.9b00920
Langmuir 2019, 35, 6708−6718

indicates that saccharide-based CDs have amphiphilic structures which help the formation of stable Langmuir monolayers. Interestingly, CDs prepared from carbon nanopowder[12] or gel-like CDs[13] did not form Langmuir monolayers, thus the amphiphilicity and ability to form a Langmuir monolayer of the saccharide-based CDs is unique.

Preparation methods of CDs are generally considered straightforward and inexpensive. In the current work, we utilized a bottom-up preparation method using hydrothermal carbonization of saccharides. CDs typically have similar optical properties regardless of their preparation methods. CDs usually have excitation-dependent PL emission.[14] Excitation-dependent emission suggests that CDs have multiple emissive centers. However, the origin of the multichromophoric units is still controversial and remains to be elucidated, although several hypotheses were proposed.[15−20] Some research groups argue that the excitation dependence results from separate particles which emit differently in the CDs population. In contrast, the excitation-dependent emission can originate from single particles with multiple emissive centers. Therefore, many studies which manipulate reaction conditions, precursor molecules, dopants,[21,22] oxidation/reduction behavior,[23] pH dependency,[24] effects of the solvents,[25] and size and surface functionalities of CDs have been studied in pursuit of enhanced understanding of the structural and optical properties of these nanoparticles. However, it is difficult to make definitive conclusions based on bulk studies as they only provide the average PL of the CDs in solution without distinguishing individual properties. Lately, single particle studies were reported to further analyze the PL of CDs which had opposing conclusions. The Langmuir monolayer technique offers a new approach to analyze the PL origin of CDs.

The Langmuir monolayer methodology is a powerful tool to study the structure and surface chemistry of materials, molecular recognition, and interactions at the membranes.[26−29] Using the Langmuir methodology, several surfactants, membrane models,[30] nanoparticles, such as quantum dots,[31,32] gold nanoparticles,[33] and soft-shell nanoparticles,[34] and graphite oxide sheets[35] have been studied. CDs have been used extensively in drug delivery[36] and biosensing,[37] although the membrane-mediated processes involved in these processes is unknown. Langmuir monolayer methodology is one of the techniques that can offer insights for membrane mimetic approaches.[38,39]

Herein, we report the first investigation of stable Langmuir monolayers of CDs. One of the two key findings of the current study is that CDs synthesized from saccharides such as lactose (LacCDs), glucose (GluCDs), and galactose (GalCDs) can reproducibly form Langmuir monolayers at the air−subphase interface. Second, PL behavior at the air−subphase interface is different than in water dispersions. These findings both provide many valuable insights about the surface characteristics of CDs and expand the understanding of the PL mechanism of CDs. This study merges two fields, namely, an emerging nanotechnology field (CDs) and a mature, well-established field (Langmuir monolayer), and therefore opens doors for new applications.

MATERIALS AND METHODS

Anhydrous D-lactose (USP/NF Grade), D-glucose, and D-galactose were purchased from MP Biomedicals, LLC (Solon, OH). The manufacturer of sodium hydroxide pellets (98.5%) (nitrogen flushed, hygroscopic) was Acros Organics. Pretreated Spectra/por7 dialysis membrane tubing, 1 kDa MWCO, was obtained from Spectrum Laboratories Supply, Inc (Rancho Dominguez, CA). Syringe filters (0.2 μm) were acquired from VWR (Radnor, PA). Deionized water (DI-H_2O) was obtained from PURELAB Ultra, ELGA LabWater (Veolia Water Solutions and Technologies, U.K.) with a resistivity of 18 MΩ·cm at 20.0 ± 0.5 °C and surface tension of 71.2 mN m^{-1} at the same temperature.

A muffle furnace (BF51800 Series) from Thermo Scientific (Rockford, IL) was utilized to run the reactions using a Teflon-coated stainless steel hydrothermal synthesis reactor from Baoshishan (DW-5MB2-BG61). A FreeZone 4.5 L cascade benchtop freeze dry system from Labconco, Co (Kansas City, MO) was used to lyophilize the samples. A Branson 1510 ultrasonicator (Gaithersburg, MD) was employed to sonicate aqueous CDs samples before characterization or Langmuir monolayer experiments.

A Cary 100 UV/vis spectrophotometer was used to obtain UV/vis absorption spectra of LacCDs dispersed in DI-H_2O using a quartz cell with 1-cm pathlength (Starna Cells, Inc). The PL emission spectra were obtained with HORIBA Jobin Yvon FluoroLog-3 (Edison, NJ) with a slit width of 5 nm for both excitation and emission. A 1 cm pathlength quartz cell was also used for the fluorescent solution measurements. Fourier transform infrared/attenuated total reflection (FTIR/ATR, PerkinElmer; Waltham, MA, USA) was used for characterization of lyophilized CDs with air as the background.

X-ray photoelectron spectra (XPS) were acquired using a PerkinElmer PHI 560 system with a double-pass cylindrical mirror analyzer using a Mg Kα anode with a $h\nu$ = 1253.6 eV photon energy operated at 250 W and 13 kV. CDs were mounted as solids onto a custom-built sample holder and inserted into the XPS system via a turbopumped antechamber. The system pressure did not exceed 1 × 10^{-8} Torr during scans. The observed C 1s core level at 284.9 eV emanating from the C═C alkenyl groups of the CDs matched with those previously measured in our laboratory;[13,40] this binding energy (BE) peak center was used as a reference. Core level intensities of the O 1s and C 1s orbitals were normalized to their known atomic sensitivity factors.[41] XPS spectra were curve-fitted using 70−30% Gaussian−Lorentzian lineshapes with Shirley background subtractions.[42] BE peak envelopes were deconvoluted using CasaXPS ver. 2.2.107 (Devonshire, UK) software.

Atomic force microscopy (AFM) (Agilent 5420 atomic force microscope with the tapping mode) and transmission electron microscopy (TEM) (a JEOL 1200× transmission electron microscope) were employed for morphological studies. ImageJ image processing program was used to measure the diameter of CDs to plot a size distribution histogram.

A syringe (100 μL) (Hamilton Co., Reno, Nevada) was used to spread CDs' aqueous dispersion on the subphase for Langmuir monolayer experiments. Kibron Micro Trough S coupled to Film Ware 2.41 software (Helsinki, Finland) was used to record surface pressure−area (π−A) and surface potential−area measurements at 19.0 ± 0.3 °C. The surface area was regulated with two symmetric computer-controlled movable barriers. The Wilhelmy method was used to measure the surface pressure employing a special alloy wire probe (diameter: 0.51 mm, sensitivity: 0.01 mN/m).

A spectrophotometer (model 8452 A HP) fixed on a rail next to KSV trough (KSV Instrument Ltd., Helsinki, Finland, dimensions: 7.5 cm × 30 cm) with a quartz window in the center was used to record the in situ UV/vis absorption spectra of CDs Langmuir monolayer. To record PL emission of CDs at the air−subphase interface, an optical fiber detector with an area of 0.25 cm^2 coupled to the Spex FluoroLog fluorescence spectrophotometer (HORIBA, Jobin Yvon, Edison, NJ) was placed on top of the KSV trough, approximately 1 mm above the surface of the subphase. In this experiment, the light from the light source is transmitted through the optical fiber to excite the Langmuir monolayer and the emitted light from the monolayer is dispatched back to the detector through the optical fiber.

The KSV trough provides plenty of space to frequently relocate the parts of the UV/vis and the fluorescence instruments as compared to the Kibron trough. Therefore, the Kibron μ-trough was employed for

DOI: 10.1021/acs.langmuir.9b00920
Langmuir 2019, 35, 6708−6718

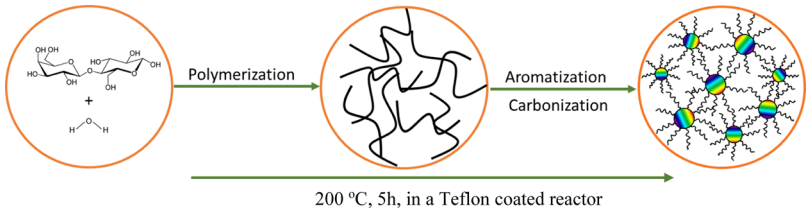

Figure 1. Schematic of the hypothesis of formation of LacCDs.

the surface pressure−potential and compression−decompression experiments and the KSV trough for in situ UV/vis and fluorescence spectroscopic experiments.

Synthesis and Characterization of CDs. CDs were prepared using D-glucose, D-galactose, or D-lactose as the carbon source via hydrothermal treatment. In a typical experiment, 20 mL of 0.3 M saccharide was transferred to a Teflon coated reactor which was placed into a muffle furnace. The reactor was heated up to 200 °C for 30 min, and the temperature was kept constant for 5 h at 200 °C. After the mixture was cooled down to room temperature, the large black chunk of solid material was removed through the centrifuge at 9000 rpm for 20 min. The supernatant was recovered and filtered through a syringe filter with a pore size of 0.2 μm to remove the insoluble fine particles. Then, the pH of the solution was adjusted to 8 using saturated NaOH aqueous solution. The solution was dialyzed against DI-H_2O for 3 days using a 1 kDa MWCO dialysis membrane changing the water every 10−12 h. Finally, the sample was lyophilized to yield the solid product.

CDs were characterized using various spectroscopic and microscopic methods such as UV/vis, fluorescence, XPS and FTIR/ATR spectroscopy, TEM, and AFM.

Langmuir Monolayer Preparation. For the Langmuir monolayer studies, 0.2 mg/mL GluCDs, GalCDs, or LacCDs' aqueous dispersions were prepared. Each experiment was repeated for two separate preparations of CDs for a minimum of two times per each batch, and good reproducibility was achieved. After the surface pressure−area measurements, LacCDs were chosen as the model and all of the following experiments at the air−subphase interphase were conducted using only LacCDs. LacCDs solution (0.2 mg/mL) was used for all other experiments. Sodium chloride solution (0.5 M) was used as the subphase. The LacCDs were spread uniformly over the air−subphase interface by using a 100 μL syringe. The spreading volume of the 0.2 mg/mL LacCDs solution was 45 μL for both surface chemistry and spectroscopic measurements at the air−subphase interface. After spreading the solution, the Langmuir monolayer was allowed to attain the equilibrium state for 10 min. Then, the monolayer was compressed at a rate of 12 $Å^2 \cdot particle^{-1} \cdot min^{-1}$ so that the compression was complete in ca. 10 min to maintain consistency in the experiments.

RESULTS AND DISCUSSION

Synthesis of Saccharide-Based Amphiphilic CDs. Hydrothermal carbonization of saccharides is a well-established method to synthesize carbon-based microspheres.[43−47] Carbon microspheres (sizes between 0.1 and 6 μm) synthesized from saccharides via hydrothermal carbonization have amphiphilic structures with a hydrophobic core and hydrophilic groups on the surface.[43,48,49] The temperature and duration of the reaction and the selected precursor and its initial concentration change the size and surface functionalities of the particles.[50,51] Also, it has been shown that with the manipulation of these parameters, the ratio of hydrophobic core to hydrophilic shell can be controlled. Studies showed that for the reactions at low temperatures carbonization does not occur.[52,53] Moreover, the larger the hydrophobic core becomes, the lesser water dispersity the particles have. We hypothesize that CDs formed during the hydrothermal treatment of saccharides with optimized conditions can also have an amphiphilic structure which can form a Langmuir monolayer. These CDs can be separated from larger microspheres formed during the reaction through a centrifuge or vacuum filtration because CDs have a high dispersity in water, whereas microspheres form insoluble, solid black chunks. Water-soluble small molecules in the crude reaction mixture can be removed via dialysis.

LacCDs were synthesized using D-lactose as the only carbon source. Under high temperature and pressure, lactose is hydrolyzed to its monosaccharide units: glucose and galactose. In the closed reaction chamber, there are many possible simultaneous reactions such as isomerization to fructose, decomposition to small organic molecules, inter- and intramolecular dehydration, aldol condensation, and/or keto−enol tautomerization reactions forming polymeric fragments and aromatic groups. When these polymeric chains reach a critical concentration in the reaction mixture, the carbonization starts forming the hydrophobic core. When the reaction is stopped, the unreacted molecules may attach on the surface giving the particles both hydrophilic and hydrophobic surface functionalities. Because of the existence of both hydrophilic and hydrophobic surface groups, saccharide-based CDs can be dispersed both in water and organic solvents with various polarities. Since lactose is a disaccharide consisting of glucose and galactose, for the formation of GluCDs and GalCDs, we propose the same route for LacCDs formation. Figure 1 summarizes the preparation of LacCDs.

Characterization of CDs. To characterize saccharide-based CDs, various spectroscopic and microscopic methods were employed. We present the results for LacCDs here. The characterization for GluCDs and GalCDs can be found in the Supporting Information (Figures S1−S3). The UV/vis absorption spectrum shows that LacCDs dispersed in water have two shoulder peaks in the 200−400 nm region, which can be attributed to $\pi-\pi^*$ (C═C) and $n-\pi^*$ (C═O) transitions (Figure 2).

LacCDs dispersed in water have excitation-dependent emission (between the blue and orange region). The PL emission of LacCDs in bulk shifts to red with the increase in the corresponding excitation wavelength. The maximum emission peak is at 445 nm when excited at 350 nm (Figure 3). The plot of normalized PL-emission spectra (inset of Figure 3) shows the emission peak maxima shift from 438 to 540 nm with respective excitation wavelengths increasing from 300 to 500 nm. The decrease in the Stokes shift from 10 507 to 1481 cm^{-1} with the longer excitation/emission wavelengths suggests that the species with longer wavelength emission are not as stable in the excited state as the species with blue emission and can be quenched more easily.

The excitation-dependent PL emission in solution can be explained in two ways: (1) There are different sized nanoparticles in the water-dispersed LacCDs population

DOI: 10.1021/acs.langmuir.9b00920
Langmuir 2019, 35, 6708−6718

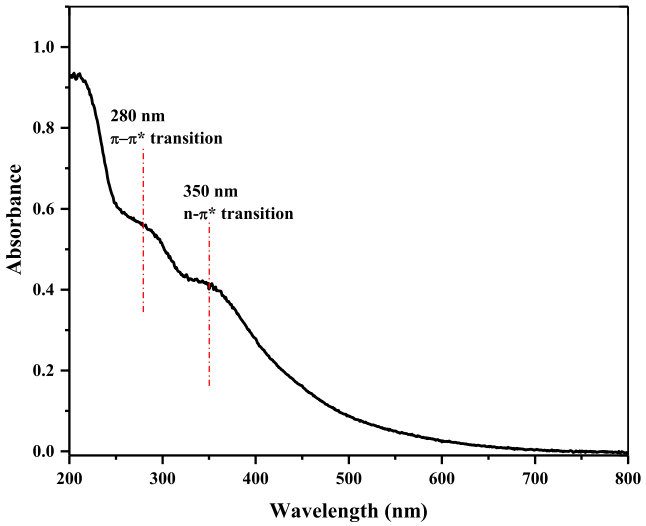

Figure 2. UV/vis absorption spectrum of LacCDs (aqueous dispersion with a concentration of 0.02 mg/mL). The $\pi-\pi^*$ transition at 280 nm is from C═C, and the $n-\pi^*$ transition at 350 nm is from C═O.

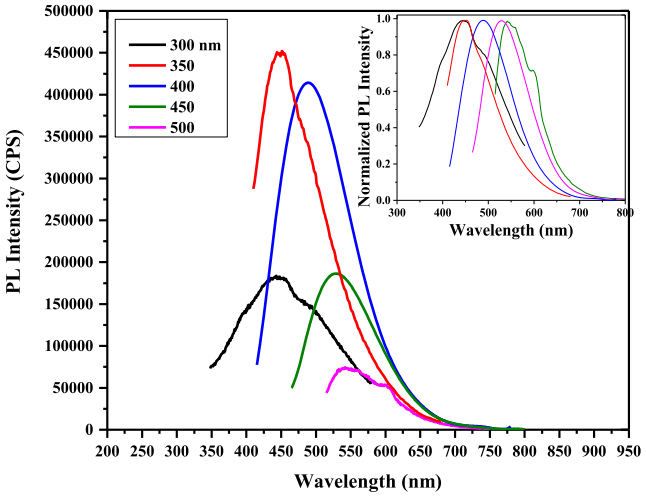

Figure 3. Excitation-dependent PL emission of 0.02 mg/mL LacCDs dispersed in water excited at 300 nm (black), 350 nm (red), 400 nm (blue), 450 nm (green), and 500 nm (pink). Maximum emission is at 445 nm, when the solution is excited at 350 nm. The inset shows the normalized PL emission spectra and the red shift of the emission with the increasing excitation wavelength.

which have different emission, and therefore, excitation dependence comes from a population of different sizes. (2) The complex surface states of LacCDs can lead to multiple electronic states. The degree and type of functionalization in CDs leads to different emissive surface states or energy traps. This accounts for the shifting of emission with excitation wavelength, as different excitation wavelengths can excite different surface states.[4,19,40,54]

FTIR/ATR studies were conducted to further characterize lyophilized LacCDs and analyze the functional groups. The spectrum shows an O−H stretch at 3330 cm^{-1}, C═O stretch at 1600 cm^{-1}, C═C stretch at 1390 cm^{-1}, and C−O stretch at 1020 cm^{-1}, consistent with the formation of hydroxyl and carboxylic functional groups (Figure 4). Figure S3 shows the FTIR spectra of GluCDs and GalCDs, which also show an O−H stretch, C═O stretch, C═C stretch, and C−O stretch in the same absorption ranges.

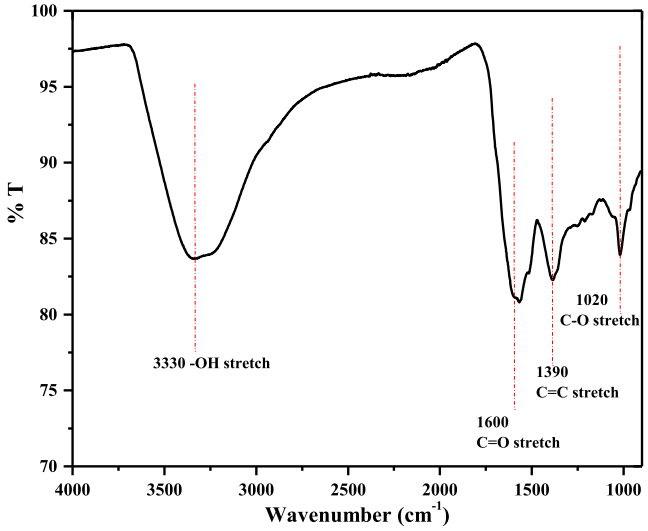

Figure 4. FTIR/ATR spectrum of lyophilized LacCDs.

Figures 5 and S4 summarize the XPS data, showing stackplots for the O 1s and C 1s core levels of the LacCDs

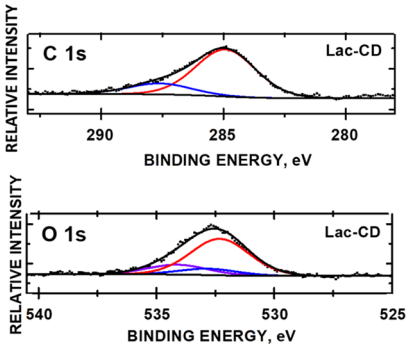

Figure 5. XPS core levels of O 1s and C 1s orbitals of LacCDs.

and GluCDs and GalCDs, respectively. Atom mole fraction results are summarized in Table S1. C 1s core level BEs for all samples were relatively constant. Although the C 1s BE at 284.9 eV matches alkenyl C (vide supra), BE at 287.6 eV is consistent with carboxylate groups (O−C═O).[55] The O 1s oxidation state at 532.8 eV is indicative of hydroxyl oxygen on the surface of the CDs.[12,13,40] Glu, Lac, and Gal CDs differ in the relative percent areas of three distinct chemical oxidation states for oxygen. The O 1s BE peak center at 534.1 eV, observed in all CD structures, is indicative of carbonyl oxygen (C═O) bound to the C dot surface,[12,13,40] with relative peak areas of 6.1, 19.1, and 3.8%, from GluCDs, LacCDs, and GalCDs, respectively. The percentage of hydroxyl oxygen (OH) present in GluCDs, LacCDs, and GalCDs were 21.6, 11.9, and 10.4%, respectively. We assign the O 1s BE peak at 532.3 eV to O groups within a polymeric backbone within the CD structure;[56] the relative O 1s peak envelope areas of this oxidation state were 72.2, 69.0, and 85.8% for the GluCDs, LacCDs, and GalCDs, respectively. Noteworthy is the fact that the C═O oxygen envelope (O 1s BE = 534.1 eV) for LacCDs (produced with a disaccharide precursor) is at least 3 times

DOI: 10.1021/acs.langmuir.9b00920
Langmuir 2019, 35, 6708−6718

greater than those of GluCDs and GalCDs, which were produced from monosaccharide precursors.

XPS data combined with FTIR/ATR confirms the formation of hydrophilic groups on the surface of the CDs. To test the amphiphilic characteristics of saccharide-based CDs, we used different organic solvents. To do this, 1 mg of the CDs were separately dispersed in 10 mL water, methanol, acetone, and tetrahydrofuran (THF), followed by fluorescence measurement. Figure S4 shows the LacCDs dispersed in water, methanol, acetone, and THF under daylight. It was observed that CDs can disperse well in methanol. However, in water and acetone, CDs precipitated minimally. Precipitation was more observable in THF. According to the fluorescence spectra of CDs dispersed in water, methanol, and acetone (Figure S5a–c), the maximum excitation wavelength shifted in different solvents from 375 (water), 425 (methanol) to 400 (acetone). The maximum emission wavelength shifted from 460 (water), 523 (methanol) to 499 (acetone), accordingly. The solvatochromic shift might be caused by solvent relaxation.[57] Also, in comparison of PL intensity in the three fluorescence spectra, it was observed that CDs might have higher dispersibility in water and methanol.[58] Therefore, compared to many CD preparations,[59] CDs made from saccharides showed more amphiphilicity.

The morphological analysis of LacCDs was performed using TEM and AFM images. Figure 6 shows a TEM image of LacCDs, and the inset shows the size distribution histogram. For each TEM measurements, a drop of the aqueous CDs solution was placed on a carbon-coated copper grid and air dried before imaging. ImageJ image processing program was used to measure the diameter of the nanoparticles which were used to plot the size histogram. The measurements from the same image were repeated three times, and a one-way repetitive ANOVA test was performed for each image. The mean CDs' diameter is 3.9 nm with a standard deviation of 1.6. Moreover, we used three additional different images and ran the one-way ANOVA test. The mean CD diameter is 4.0 nm with a standard deviation of 1.8. Based on the TEM images and size distribution analysis, LacCDs have a narrow size distribution with most particles having a diameter between 2.2 and 5.8 nm.

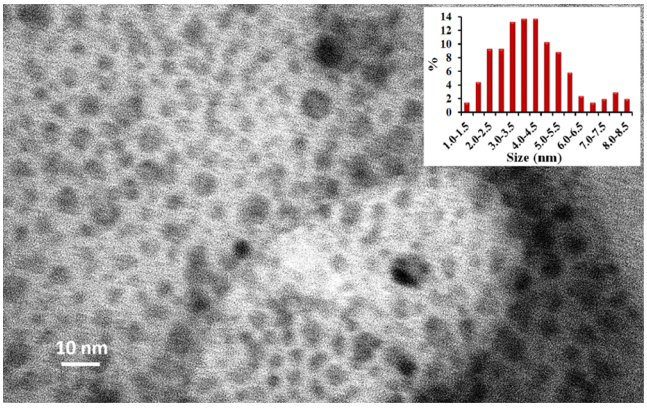

Figure 6. TEM image of LacCDs. The inset shows the size distribution histogram.

AFM samples were prepared by placing approximately 20 μL of aqueous CDs solution on a clean mica slide and air dried. This was then placed under the AFM tip and imaged using the tapping mode. The AFM tip was a silicon tip (length: 225 μm; thickness: 5 μm) with a force constant of 15 N/m. The AFM image of LacCDs (Figure 7A) shows both the LacCD particles well dispersed in water, and two areas of cluster formation. The areas shown in red dashed lines (Figure 7A) were zoomed-in to show an agglomerate (Figure 7B) and a well-dispersed area (Figure 7C). The extracted profile from the well-dispersed area (Figure 7C) shows particle heights less than 3.5 nm. Given that the mean diameter of CDs is 4.0 ± 1.8 nm based on the TEM images, LacCDs have a spherical shape. The larger height (7 nm), shown from the profile of the agglomerated area, results from the crowding of the nanoparticles, so that they begin to overlap. The zeta potential (−21.8 ± 0.3 mV) of LacCDs is consistent with their tendency to form agglomerates in aqueous solution. The low absolute value of zeta potential means weaker repulsive interactions between the nanoparticles, which is consistent with the hypothesis that LacCDs can stick together to form a Langmuir monolayer. To avoid 3D clustering of LacCDs in the Langmuir monolayer studies, the sample solution is sonicated (with a frequency of 42 kHz) for 10–15 min right before spreading on the subphase of the Langmuir trough.

Surface Pressure and Surface Potential Versus Area Isotherms. The Langmuir monolayer technique was used to study the two-dimensional (2D) behavior of LacCDs at the air–subphase interface. A stable monolayer was obtained by spreading 45 μL of 0.2 mg/mL LacCDs dispersed in DI-H_2O on the surface of a 0.5 M NaCl subphase. The reason for using a 0.5 M NaCl as a subphase is to neutralize the LacCDs' ionic surface groups. Strong hydrogen bonds at the air–subphase

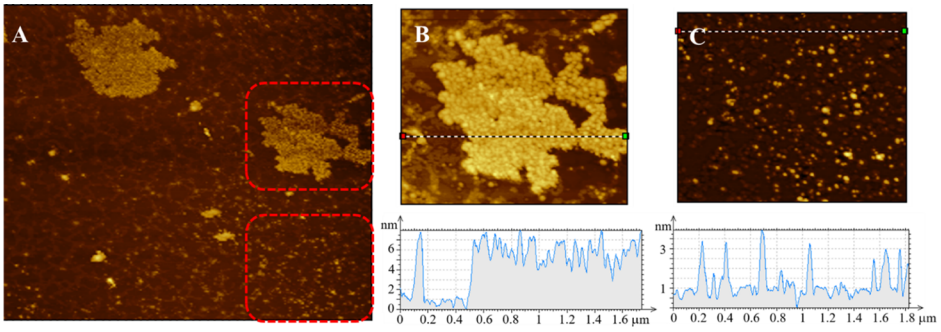

Figure 7. AFM image of LacCDs (A) Zoomed-in image of an agglomerated area (top) and the extracted profile (bottom), (B) Zoomed-in image of the well-dispersed LacCDs (top) and the extracted profile (bottom), and (C) Dashed lines on images B and C show the area where the particles are extracted to show the height distribution.

DOI: 10.1021/acs.langmuir.9b00920
Langmuir 2019, 35, 6708–6718

interface help stabilize the CDs to form a Langmuir monolayer. Lower concentrations of the NaCl (0.1 M) subphase did not have enough counterions for LacCDs. Hence, we did not observe the formation of a Langmuir monolayer. The experiments were repeated at least three times using different synthesis batches of LacCDs. Aqueous dispersion of LacCDs (0.2 mg/mL) showed reproducibly the formation of the essential phases of 2D LacCD Langmuir monolayer. We also showed that the CDs from the two moieties of lactose (glucose and galactose) also form a Langmuir monolayer (Figures S7 and S8). We continued only with LacCDs (0.2 mg/mL) to further study Langmuir monolayer properties because the π–A curve of the LacCD monolayer had a higher collapse pressure and, thus, had a higher stability. The Langmuir monolayer of LacCDs is better suited for UV/vis absorption and PL emission as these experiments last longer and require a more stable monolayer. Also, with the larger collapse pressure, the essential phases of the Langmuir monolayer of LacCDs were more distinguished as compared to GluCDs and GalCDs. Other than the different average size, LacCDs have the same optical properties as GluCDs and GalCDs in aqueous dispersion. Therefore, the Langmuir monolayer of LacCDs was selected as a model system for further experimentation.

Surface pressure–area (π–A) and surface potential–area isotherms are shown in Figure 8. Surface pressure isotherm can

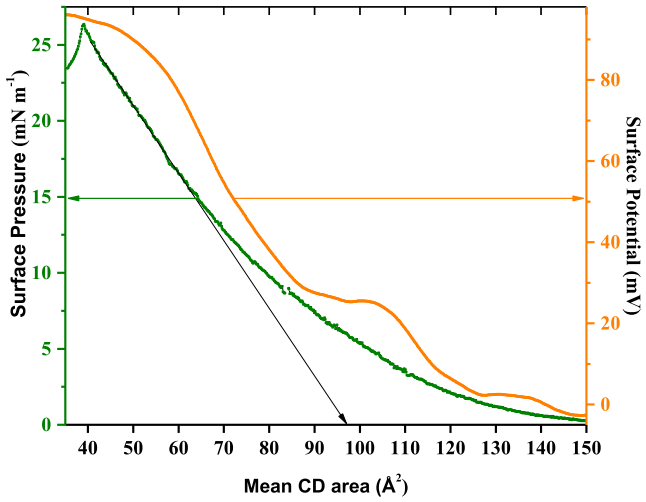

Figure 8. Surface pressure–area (green) and surface potential–area (orange) isotherms of LacCDs (0.2 mg/mL aqueous dispersion). The figure also shows the corresponding phase changes.

be used to analyze the interactions between particles in close proximity (van der Waals interaction), whereas surface potential can aid in understanding the interactions between particles at longer distances (dipole–dipole interaction). The initial zero surface pressure above 150 Å^2/LacCD corresponds to the gaseous phase. In the gaseous phase, the LacCD particles have little to zero interaction. As the nanoparticles move closer because of the compression from the moving barriers, the surface pressure increases along with the phase change from gas to liquid, and then to solid. The LacCD Langmuir monolayer collapses above 25 mN/m. Each change in the slope of the π–A curve corresponds to a phase change, namely, liquid-expanded (LE) from 150 to about 100 Å^2/LacCD, liquid-condensed (LC) from 100 to 62 Å^2/LacCD, and solid phases covering the region from 62 to about 40 Å^2/LacCD. As the phases change from gas to liquid and eventually solid, the LacCD nanoparticles are less free to move, and the orientation of the particles becomes more uniform and rigid. Because the exact structure of CDs is not known even if the LacCDs have a spherical shape, the surface functionalities may not be uniform. In a close-packed Langmuir monolayer, the more polar surface groups are expected to face to the polar subphase whereas the nonpolar or less polar groups are expected to face to air. This alignment is more favored because the counterions (Na^+ and Cl^-) of the subphase have stronger interactions with polar groups of LacCDs, resulting in a more stable Langmuir monolayer.

The limiting CD area for LacCDs is found by extrapolating the linear part of the π–A isotherm to zero pressure and taking the value of the CD area at the interception.[31,32] Figure 8 shows a limiting CD area of 97 Å^2 for LacCDs. Because LacCDs are spherical nanoparticles, the limiting LacCD area, which provide the cross-sectional area of the particle, can be utilized to estimate the diameter of the LacCDs at the monolayer. The area of the circle formula (πr^2) was used to calculate the radius and the diameter of CDs at the monolayer.[31,32] LacCDs have a diameter of 1.1 nm in a close-packed, rigid monolayer. Difference between the average particle size based on the TEM and AFM images (~4 nm) and Langmuir monolayers may be due to the particles being in a more relaxed state in solution in contrast to the close-packed in monolayers. On the other hand, knowing that the LacCDs easily form clusters in solution, the higher size distribution from TEM could be an inflated average diameter resulting from agglomerates. The TEM image (Figure S9) shows clearly that smaller LacCD particles migrate together and start forming an agglomerate.

The limiting CD area of GluCDs (Figure S7) and GalCDs (Figure S8) are 53 and 49.5 Å^2/CD, respectively, and smaller than LacCDs. Therefore, the calculated diameter of both GluCDs and GalCDs at the close-packed Langmuir monolayer is ~0.8 nm. This result is consistent with the hypothesis that starting with a smaller precursor molecule, and keeping rest of the parameters of reaction constant, yields CDs with smaller diameters. Furthermore, it confirms that CDs from glucose and galactose have the same sizes since the precursors are isomers.

The surface potential versus area isotherm is shown in the orange curve (Figure 8). Surface potential displays the potential difference between the subphase and air (above and below the Langmuir monolayer film). In other words, it displays the difference in dipole moments. Furthermore, surface potential can be used to evaluate the molecular interactions which occur during phase change of the monolayer. The bumps seen in the LE and LC phases are due to the molecular motions and rearrangements of LacCDs to gain specific orientations corresponding to each phase change. On the other hand, the bumps observed at about 130 and 95 Å^2/LacCD might be due to a different aggregation state in the Langmuir monolayer. It must be noted that there is a good correlation between the surface pressure and surface potential isotherms. The maximum voltage of about 100 mV is consistent with compact packing of LacCD nanoparticles at the air–subphase interface.

We were further interested to know the rigidity of the Langmuir monolayer of LacCDs and its robustness. Hence, compression modulus of the π–A isotherm was plotted as a function of surface pressure as shown in Figure 9. The compression modulus was determined by using the equation

DOI: 10.1021/acs.langmuir.9b00920
Langmuir 2019, 35, 6708–6718

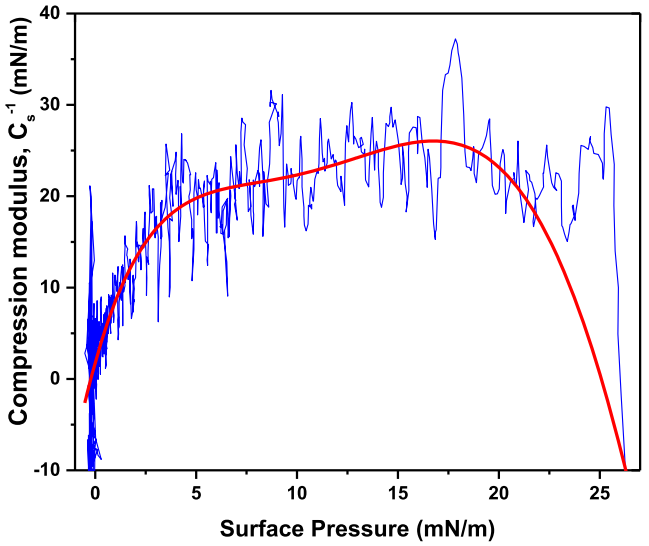

Figure 9. Compression modulus as a function of surface pressure (π).

$C_s^{-1} = -A\, d\pi/dA$,[60,61] where C_s is the compression modulus, π is the surface pressure, and A is the mean LacCD area based on π–A curve data. In Figure 8, the surface pressure of 17 mN/m corresponds to the change from LC to S phase. This surface pressure coincides with the maximum compression modulus (Figure 9). This phenomenon can be explained on the basis of maximum repulsive forces between the LacCDs at the interface.

Compression–Decompression Cycles and Stability. Compression–decompression experiments were conducted to test the stability of the LacCD Langmuir monolayer. Figure 10

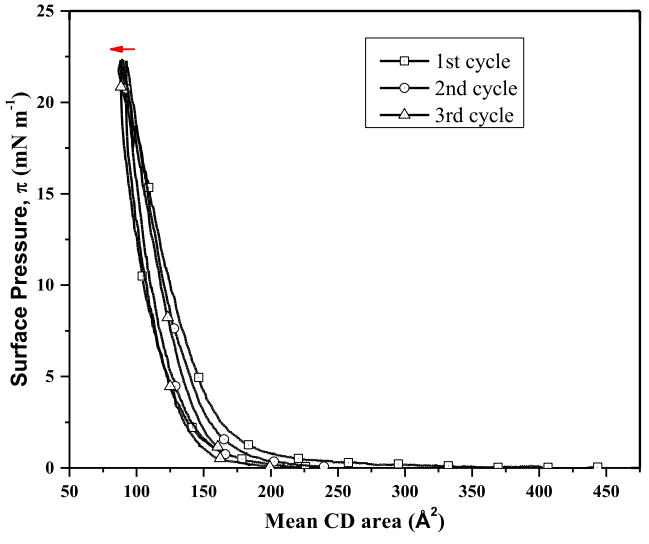

Figure 10. Compression–decompression curves of the LacCD Langmuir monolayer.

shows the three compression–decompression cycles. After the experiment, the average hysteresis was obtained as 4.3%. The Langmuir monolayer shows minimum hysteresis confirming the retaining ability of the nanoparticles at the air–subphase interface. Furthermore, the hysteresis data gives the information that LacCDs reorganized at the air–subphase interface, whereas the 0.5 M NaCl subphase solution provides the partial insolubility of LacCDs at the interface.

To further assess the stability of the LacCD Langmuir monolayer, we performed an additional stability study. After spreading the LacCDs dispersion on the subphase, movable barriers were used to compress the monolayer to a surface pressure of 12 mN/m. Then, the barriers were stopped to maintain the surface pressure. Figure 11 shows the mean

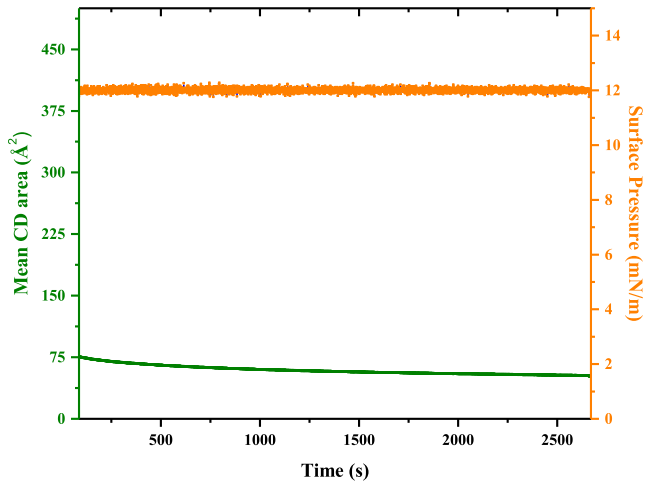

Figure 11. Stability study of the LacCD Langmuir monolayer confirms that LacCDs can retain in the monolayer for the duration that is necessary for spectroscopic studies.

LacCD area at the interface and the stable surface pressure for about 45 min. This means that LacCDs are stable enough to retain in the monolayer at the air–subphase interphase for the whole time necessary for the in situ spectroscopic recordings.

UV/Vis Absorption at the Air–Subphase Interface. Figure 12 shows the UV/vis absorption spectra of the LacCD monolayer at different surface pressures. This experiment lets us explore the extent of the analyte that remains on the monolayer with increasing surface pressure. As expected for a stable monolayer, the intensity of absorbance at the peak maximum increases with increasing surface pressure as the nanoparticles come closer with increased compression. The

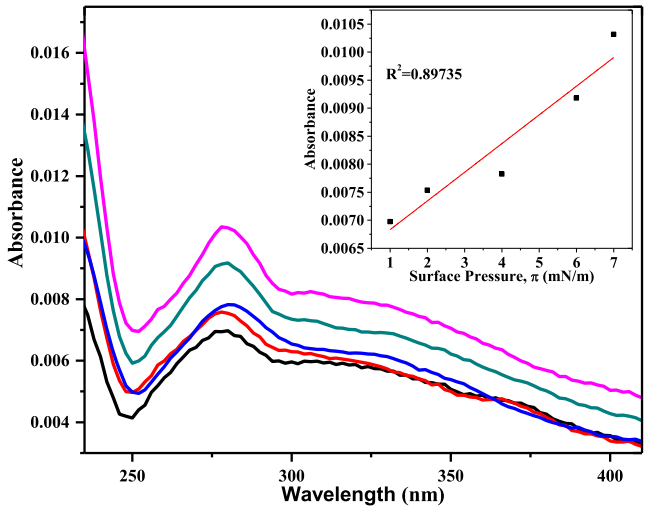

Figure 12. UV/vis absorption spectra of the LacCD Langmuir monolayer at different surface pressures. Surface pressure is 1 (black), 2 (red), 4 (blue), 6 (green), and 7 (pink) mN/m. The inset shows the linear increase in the absorbance maxima at 280 nm.

DOI: 10.1021/acs.langmuir.9b00920
Langmuir 2019, 35, 6708–6718

inset of Figure 12 shows the linear increase of absorbance maxima at 280 nm with increasing surface pressure. This result further confirms the stability of the LacCD monolayer. UV/vis absorption spectra of LacCDs as a dispertion and in monolayer at the air−subphase interface have the same shoulder peaks at 280 and 350 nm. This result shows that the aggregation in 2D is not an important factor because we do not observe any red shift in the absorption spectrum of the Langmuir monolayer. It is reasonable that the peak at 350 nm is not as pronounced in the monolayer as in solution because the intensity of absorption is much smaller from a Langmuir monolayer as compared to bulk solution.

PL of the LacCD Langmuir Monolayer. To investigate PL properties of LacCD monolayers, the monolayer was first excited at 280 nm. Figure 13 shows the PL emission spectra of

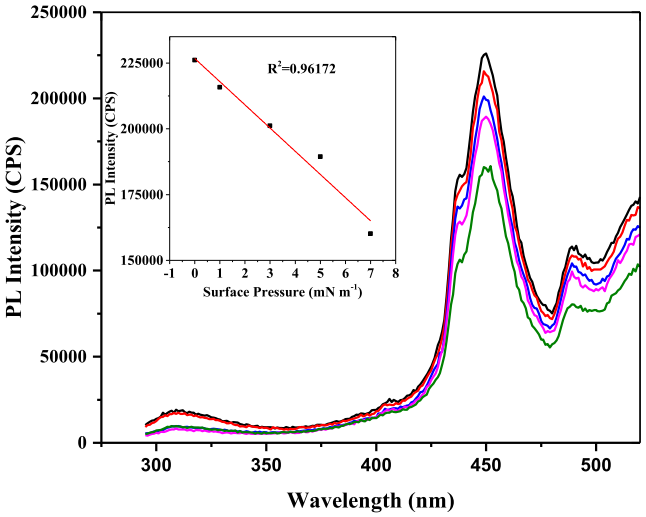

Figure 13. PL emission spectra of the LacCD Langmuir monolayer at different surface pressures when excited at 280 nm. Surface pressure is 0 (black), 1 (red), 3 (blue), 5 (pink), and 7 (green) mN/m. The inset shows the linear decrease in the PL maxima at 460 nm when excited at 280 nm.

the LacCD monolayer at different surface pressures (0, 1, 3, 5, and 7 mN m^{-1}) when excited at 280 nm. The intensity of the emission peak decreases with increasing surface pressure. This self-quenching of emission may be due to the processes that compete with fluorescence, such as Förster resonance energy transfer (FRET). When the nanoparticles move closer with increased surface pressure, this competitive process becomes more dominant and therefore the intensity of fluorescence decreases. The inset of Figure 13 shows the linear decrease in the PL intensity with increasing surface pressure when excited at 280 nm. It should be stated that the intensity of PL emission of LacCDs dispersed in water also decreases in higher concentrations. Figure S10 shows the increase in the PL intensity in solution with increasing concentration until the maximum of 0.02 mg/mL. For the concentrations more than 0.02 mg/mL, quenching starts and intensity of PL decreases with increasing concentration of LacCDs. Increasing concentration in solution can be comparable to the increasing surface pressure in the Langmuir trough because increase in both concentration and surface pressure results in closer distances between particles. The self-quenching starts in both the solution and Langmuir monolayer when LacCDs are crowded.

Next, the LacCD monolayer is excited at different wavelengths (350, 380, and 400 nm) and PL emission at the air−subphase interface is recorded at the same surface pressure (4 mN m^{-1}). Figure 14 shows that the PL emission of the

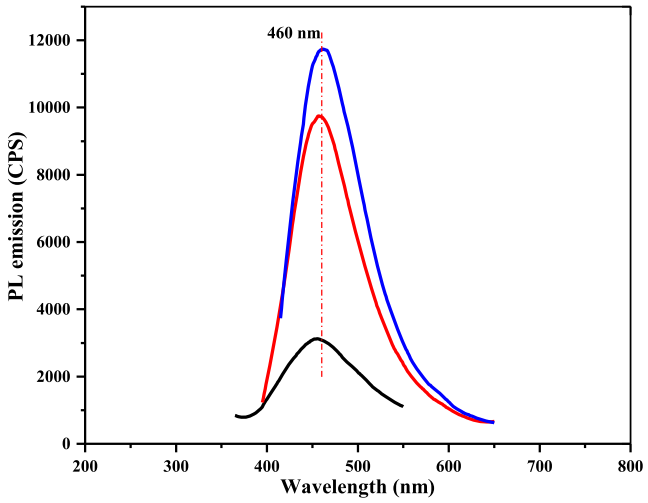

Figure 14. Excitation-independent PL emission spectra of the LacCD Langmuir monolayer at the air−subphase interface. The Langmuir monolayer of LacCDs is excited at 350 (black), 380 (red), and 400 (blue) nm and emission with a maximum at 460 nm is recorded at the same surface pressure of 4 mN m^{-1}.

LacCD monolayer is excitation independent in contrast to the excitation-dependent PL in aqueous dispersion. PL emission with varying excitation wavelengths at different surface pressures (2 and 6 mN m^{-1}) also showed the same excitation-independent spectra (Figures S11 and S12). The PL emission maximum at the air−subphase interface is at 460 nm regardless of the excitation wavelength. PL maximum in aqueous dispersion is at 445 nm when excited at 350 nm. Interestingly, the maximum intensity of PL at the air−subphase interface is when the monolayer is excited at 400 nm. The PL peak is at 487 nm when excited at 400 nm in aqueous dispersion whereas it is at 460 nm at the air−subphase interface.

The excitation-independent emission of the LacCD monolayer might stem from the complex surface states rather than the size of CDs. This can be explained by the significantly more uniform orientation of LacCD nanoparticles in the Langmuir monolayer compared to that in the aqueous dispersion. When LacCDs are dispersed in water, different emitting, complex surface states contribute to the excitation-dependent PL emission. However, in a 2D monolayer, the surface states with similar properties align in a specific direction giving the monolayer a more uniform emission. In Langmuir monolayers, the nanoparticles orient themselves in such a way where more polar groups are stabilized by the counterions of subphase and the nonpolar/less polar groups mainly face the air. Also, the conformation of the surface functional groups might change in a rigid, close-packed Langmuir monolayer due to steric hindrance compared to the bulk. The rearrangement and change in the conformation of surface moieties may result in new electronic states or a change in energy levels between ground and excited states. Therefore, for the PL maxima at the air−subphase interface, we observe a red shift for shorter excitation wavelengths (Stokes shift increases from 6100 to 6832 cm^{-1}) and a blue

DOI: 10.1021/acs.langmuir.9b00920
Langmuir 2019, 35, 6708−6718

shift for longer excitation wavelengths (Stokes shift decreases from 4466 to 3260 cm^{-1}) when compared to PL maxima in solution. Slight difference in Stokes shifts in solution and at the air−subphase interface suggests that there is a change in the difference between ground and excited state dipole moments. Considering that CDs dispersed in water form the Langmuir monolayer when spread on the subphase regardless of their size and also LacCDs have a narrow size distribution, population-based excitation-dependent emission, namely, the quantum confinement effect is less likely the origin of PL emission of LacCDs.

CONCLUSIONS

In conclusion, we successfully and reproducibly showed, for the first-time, formation of stable Langmuir monolayers of CDs. Photoluminescent CDs were prepared using saccharides (lactose, glucose, and galactose) as the carbon source via a bottom up method. π−A and surface potential isotherms show stable monolayers and characteristic phase changes of LacCD monolayers. Compression−decompression studies showed minimum hysteresis confirming the stability of the LacCD monolayer. Furthermore, LacCD monolayers exhibited an excitation-independent PL, whereas PL emission of LacCDs dispersed in water is excitation dependent. The intensity of the emission peak of LacCD monolayers decreases with increasing surface pressure when excited at 280 nm, suggesting the possibility of FRET at the air−subphase interface.

The ability to form stable Langmuir monolayers combined with the unique optical properties of CDs not only improves the understanding of the structure and PL mechanism of CDs, but also extends areas for future applications and introduces a new important direction of the interface science and colloid chemistry.

ASSOCIATED CONTENT

Supporting Information

The Supporting Information is available free of charge on the ACS Publications website at DOI: 10.1021/acs.langmuir.9b00920.

UV/vis absorption, PL, FTIR, and XPS spectra of GluCDs and GalCDs, elemental atom % analysis of GluCDs and GalCDs, photograph of LacCDs dispersed in different solvents under day light, PL spectra of LacCDs in various solvents, π A isotherms of GluCD and GalCD Langmuir monolayers, TEM image of LacCDs agglomerate, concentration-dependent PL of LacCDs' aqueous dispersion, and excitation-independent PL spectra of LacCD Langmuir monolayer at different surface pressures (PDF)

AUTHOR INFORMATION

Corresponding Author

*E-mail: rml@miami.edu.

ORCID

Yiqun Zhou: 0000-0002-6594-9925

Charles C. Chusuei: 0000-0002-1283-4980

Roger M. Leblanc: 0000-0001-8836-8042

Notes

The authors declare no competing financial interest.

ACKNOWLEDGMENTS

R.M.L. gratefully acknowledges the support of the National Science Foundation grant 011298 and National Institute of Health grant 009887.

REFERENCES

(1) Xu, X.; Ray, R.; Gu, Y.; Ploehn, H. J.; Gearheart, L.; Raker, K.; Scrivens, W. A. Electrophoretic analysis and purification of fluorescent single-walled carbon nanotube fragments. *J. Am. Chem. Soc.* **2004**, *126*, 12736−12737.

(2) Sun, Y.-P.; Zhou, B.; Lin, Y.; Wang, W.; Fernando, K. A. S.; Pathak, P.; Meziani, M. J.; Harruff, B. A.; Wang, X.; Wang, H.; Luo, P. G.; Yang, H.; Kose, M. E.; Chen, B.; Veca, L. M.; Xie, S.-Y. Quantum-sized carbon dots for bright and colorful photoluminescence. *J. Am. Chem. Soc.* **2006**, *128*, 7756−7757.

(3) Yang, S.-T.; Cao, L.; Luo, P. G.; Lu, F.; Wang, X.; Wang, H.; Meziani, M. J.; Liu, Y.; Qi, G.; Sun, Y.-P. Carbon dots for optical imaging in vivo. *J. Am. Chem. Soc.* **2009**, *131*, 11308−11309.

(4) Zhu, S.; Meng, Q.; Wang, L.; Zhang, J.; Song, Y.; Jin, H.; Zhang, K.; Sun, H.; Wang, H.; Yang, B. Highly photoluminescent carbon dots for multicolor patterning, sensors, and bioimaging. *Angew. Chem.* **2013**, *125*, 4045−4049.

(5) Zheng, X. T.; Ananthanarayanan, A.; Luo, K. Q.; Chen, P. Glowing graphene quantum dots and carbon dots: properties, syntheses, and biological applications. *Small* **2015**, *11*, 1620−1636.

(6) Jia, X.; Li, J.; Wang, E. One-pot green synthesis of optically pH-sensitive carbon dots with upconversion luminescence. *Nanoscale* **2012**, *4*, 5572−5575.

(7) Yang, S.-T.; Wang, X.; Wang, H.; Lu, F.; Luo, P. G.; Cao, L.; Meziani, M. J.; Liu, J.-H.; Liu, Y.; Chen, M.; Huang, Y.; Sun, Y.-P. Carbon dots as nontoxic and high-performance fluorescence imaging agents. *J. Phys. Chem. C* **2009**, *113*, 18110−18114.

(8) Hola, K.; Zhang, Y.; Wang, Y.; Giannelis, E. P.; Zboril, R.; Rogach, A. L. Carbon dots-Emerging light emitters for bioimaging, cancer therapy and optoelectronics. *Nano Today* **2014**, *9*, 590−603.

(9) Agina, E. V.; Mannanov, A. A.; Sizov, A. S.; Vechter, O.; Borshchev, O. V.; Bakirov, A. V.; Shcherbina, M. A.; Chvalun, S. N.; Konstantinov, V. G.; Bruevich, V. V.; Kozlov, O. V.; Pshenichnikov, M. S.; Paraschuk, D. Y.; Ponomarenko, S. A. Luminescent organic semiconducting langmuir monolayers. *ACS Appl. Mater. Interfaces* **2017**, *9*, 18078−18086.

(10) Bhunia, S. K.; Maity, A. R.; Nandi, S.; Stepensky, D.; Jelinek, R. Imaging cancer cells expressing the folate receptor with carbon dots produced from folic acid. *ChemBioChem* **2016**, *17*, 614−619.

(11) Zheng, M.; Ruan, S.; Liu, S.; Sun, T.; Qu, D.; Zhao, H.; Xie, Z.; Gao, H.; Jing, X.; Sun, Z. Self-targeting fluorescent carbon dots for diagnosis of brain cancer cells. *ACS Nano* **2015**, *9*, 11455−11461.

(12) Li, S.; Wang, L.; Chusuei, C. C.; Suarez, V. M.; Blackwelder, P. L.; Micic, M.; Orbulescu, J.; Leblanc, R. M. Nontoxic carbon dots potently inhibit human insulin fibrillation. *Chem. Mater.* **2015**, *27*, 1764−1771.

(13) Zhou, Y.; Desserre, A.; Sharma, S. K.; Li, S.; Marksberry, M. H.; Chusuei, C. C.; Blackwelder, P. L.; Leblanc, R. M. Gel-like Carbon Dots: Characterization and their Potential Applications. *ChemPhysChem* **2017**, *18*, 890−897.

(14) Dong, Y.; Pang, H.; Yang, H. B.; Guo, C.; Shao, J.; Chi, Y.; Li, C. M.; Yu, T. Carbon-Based Dots Co-doped with Nitrogen and Sulfur for High Quantum Yield and Excitation-Independent Emission. *Angew. Chem.* **2013**, *125*, 7954−7958.

(15) Zhu, S.; Song, Y.; Zhao, X.; Shao, J.; Zhang, J.; Yang, B. The photoluminescence mechanism in carbon dots (graphene quantum dots, carbon nanodots, and polymer dots): current state and future perspective. *Nano Res.* **2015**, *8*, 355−381.

(16) Zhu, S.; Zhang, J.; Tang, S.; Qiao, C.; Wang, L.; Wang, H.; Liu, X.; Li, B.; Li, Y.; Yu, W.; Wang, X.; Sun, H.; Yang, B. Surface Chemistry Routes to Modulate the Photoluminescence of Graphene Quantum Dots: From Fluorescence Mechanism to Up-Conversion Bioimaging Applications. *Adv. Funct. Mater.* **2012**, *22*, 4732−4740.

DOI: 10.1021/acs.langmuir.9b00920
Langmuir 2019, 35, 6708−6718

(17) Xu, Q.; Kuang, T.; Liu, Y.; Cai, L.; Peng, X.; Sreenivasan Sreeprasad, T.; Zhao, P.; Yu, Z.; Li, N. Heteroatom-doped carbon dots: synthesis, characterization, properties, photoluminescence mechanism and biological applications. *J. Mater. Chem. B* **2016**, *4*, 7204−7219.
(18) Hola, K.; Bourlinos, A. B.; Kozak, O.; Berka, K.; Siskova, K. M.; Havrdova, M.; Tucek, J.; Safarova, K.; Otyepka, M.; Giannelis, E. P.; Zboril, R. Photoluminescence effects of graphitic core size and surface functional groups in carbon dots: COO− induced red-shift emission. *Carbon* **2014**, *70*, 279−286.
(19) Wen, Z.-H.; Yin, X.-B. Excitation-independent carbon dots, from photoluminescence mechanism to single-color application. *RSC Adv.* **2016**, *6*, 27829−27835.
(20) Fang, Q.; Dong, Y.; Chen, Y.; Lu, C.-H.; Chi, Y.; Yang, H.-H.; Yu, T. Luminescence origin of carbon based dots obtained from citric acid and amino group-containing molecules. *Carbon* **2017**, *118*, 319−326.
(21) Xu, Y.; Wu, M.; Liu, Y.; Feng, X.-Z.; Yin, X.-B.; He, X.-W.; Zhang, Y.-K. Nitrogen-Doped Carbon Dots: A Facile and General Preparation Method, Photoluminescence Investigation, and Imaging Applications. *Chem.—Eur. J.* **2013**, *19*, 2276−2283.
(22) Lu, W.; Gong, X.; Nan, M.; Liu, Y.; Shuang, S.; Dong, C. Comparative study for N and S doped carbon dots: synthesis, characterization and applications for Fe^{3+} probe and cellular imaging. *Anal. Chim. Acta* **2015**, *898*, 116−127.
(23) Xu, Y.; Wu, M.; Feng, X.-Z.; Yin, X.-B.; He, X.-W.; Zhang, Y.-K. Reduced Carbon Dots versus Oxidized Carbon Dots: Photo- and Electrochemiluminescence Investigations for Selected Applications. *Chem.—Eur. J.* **2013**, *19*, 6282−6288.
(24) Pan, D.; Zhang, J.; Li, Z.; Wu, C.; Yan, X.; Wu, M. Observation of pH-, solvent-, spin-, and excitation-dependent blue photoluminescence from carbon nanoparticles. *Chem. Commun.* **2010**, *46*, 3681−3683.
(25) Wang, F.; Pang, S.; Wang, L.; Li, Q.; Kreiter, M.; Liu, C.-y. One-step synthesis of highly luminescent carbon dots in noncoordinating solvents. *Chem. Mater.* **2010**, *22*, 4528−4530.
(26) Brezesinski, G.; Möhwald, H. Langmuir monolayers to study interactions at model membrane surfaces. *Adv. Colloid Interface Sci.* **2003**, *100-102*, 563−584.
(27) Kaganer, V. M.; Möhwald, H.; Dutta, P. Structure and phase transitions in Langmuir monolayers. *Rev. Mod. Phys.* **1999**, *71*, 779−819.
(28) Landau, E. M.; Levanon, M.; Leiserowitz, L.; Lahav, M.; Sagiv, J. Transfer of structural information from Langmuir monolayers to three-dimensional growing crystals. *Nature* **1985**, *318*, 353−356.
(29) Leblanc, R. Molecular recognition at Langmuir monolayers. *Curr. Opin. Chem. Biol.* **2006**, *10*, 529−536.
(30) Stefaniu, C.; Brezesinski, G.; Möhwald, H. Langmuir monolayers as models to study processes at membrane surfaces. *Adv. Colloid Interface Sci.* **2014**, *208*, 197−213.
(31) Ji, X.; Wang, C.; Xu, J.; Zheng, J.; Gattás-Asfura, K. M.; Leblanc, R. M. Surface Chemistry Studies of (CdSe)ZnS Quantum Dots at the Air−Water Interface. *Langmuir* **2005**, *21*, 5377−5382.
(32) Gattás-Asfura, K. M.; Constantine, C. A.; Lynn, M. J.; Thimann, D. A.; Ji, X.; Leblanc, R. M. Characterization and 2D Self-Assembly of CdSe Quantum Dots at the Air−Water Interface. *J. Am. Chem. Soc.* **2005**, *127*, 14640−14646.
(33) Schultz, D. G.; Lin, X.-M.; Li, D.; Gebhardt, J.; Meron, M.; Viccaro, J.; Lin, B. Structure, wrinkling, and reversibility of Langmuir monolayers of gold nanoparticles. *J. Phys. Chem. B* **2006**, *110*, 24522−24529.
(34) El-Tawargy, A. S.; Stock, D.; Gallei, M.; Ramadan, W. A.; Shams El-Din, M. A.; Reiter, G.; Reiter, R. Multiple structural transitions in Langmuir monolayers of charged soft-shell nanoparticles. *Langmuir* **2018**, *34*, 3909−3917.
(35) Cote, L. J.; Kim, F.; Huang, J. Langmuir− Blodgett assembly of graphite oxide single layers. *J. Am. Chem. Soc.* **2008**, *131*, 1043−1049.
(36) Wang, Q.; Huang, X.; Long, Y.; Wang, X.; Zhang, H.; Zhu, R.; Liang, L.; Teng, P.; Zheng, H. Hollow luminescent carbon dots for drug delivery. *Carbon* **2013**, *59*, 192−199.
(37) Kong, B.; Zhu, A.; Ding, C.; Zhao, X.; Li, B.; Tian, Y. Carbon Dot-Based Inorganic-Organic Nanosystem for Two-Photon Imaging and Biosensing of pH Variation in Living Cells and Tissues. *Adv. Mater.* **2012**, *24*, 5844−5848.
(38) Sharma, S. K.; Seven, E. S.; Micic, M.; Li, S.; Leblanc, R. M. Surface chemistry and spectroscopic study of a cholera toxin B Langmuir monolayer. *Langmuir* **2018**, *34*, 2557−2564.
(39) Sharma, S. K.; Li, S.; Micic, M.; Orbulescu, J.; Weissbart, D.; Nakahara, H.; Shibata, O.; Leblanc, R. M. β-Galactosidase Langmuir Monolayer at Air/X-gal Subphase Interface. *J. Phys. Chem. B* **2016**, *120*, 12279−12286.
(40) Zhou, Y.; Liyanage, P. Y.; Geleroff, D. L.; Peng, Z.; Mintz, K. J.; Hettiarachchi, S. D.; Pandey, R. R.; Chusuei, C. C.; Blackwelder, P. L.; Leblanc, R. M. Photoluminescent carbon dots: A mixture of heterogeneous fractions. *ChemPhysChem* **2018**, *19*, 2589−2597.
(41) Wagner, C. D.; Davis, L. E.; Zeller, M. V.; Taylor, J. A.; Raymond, R. H.; Gale, L. H. Empirical atomic sensitivity factors for quantitative analysis by electron spectroscopy for chemical analysis. *Surf. Interface Anal.* **1981**, *3*, 211−225.
(42) Shirley, D. A. High-resolution X-ray photoemission spectrum of the valence bands of gold. *Phys. Rev. B* **1972**, *5*, 4709−4714.
(43) Sevilla, M.; Fuertes, A. B. The production of carbon materials by hydrothermal carbonization of cellulose. *Carbon* **2009**, *47*, 2281−2289.
(44) Kang, S.; Li, X.; Fan, J.; Chang, J. Characterization of hydrochars produced by hydrothermal carbonization of lignin, cellulose, D-xylose, and wood meal. *Ind. Eng. Chem. Res.* **2012**, *51*, 9023−9031.
(45) Tran, H. N.; Lee, C.-K.; Nguyen, T. V.; Chao, H.-P. Saccharide-derived microporous spherical biochar prepared from hydrothermal carbonization and different pyrolysis temperatures: synthesis, characterization, and application in water treatment. *Environ. Technol.* **2018**, *39*, 2747−2760.
(46) Aydıncak, K.; Yumak, T. r.; Sınağ, A.; Esen, B. Synthesis and characterization of carbonaceous materials from saccharides (glucose and lactose) and two waste biomasses by hydrothermal carbonization. *Ind. Eng. Chem. Res.* **2012**, *51*, 9145−9152.
(47) Ryu, J.; Suh, Y.-W.; Suh, D. J.; Ahn, D. J. Hydrothermal preparation of carbon microspheres from mono-saccharides and phenolic compounds. *Carbon* **2010**, *48*, 1990−1998.
(48) Sun, X.; Li, Y. Colloidal Carbon Spheres and Their Core/Shell Structures with Noble-Metal Nanoparticles. *Angew. Chem.* **2004**, *116*, 607−611.
(49) Shin, Y.; Wang, L.-Q.; Bae, I.-T.; Arey, B. W.; Exarhos, G. J. Hydrothermal syntheses of colloidal carbon spheres from cyclodextrins. *J. Phys. Chem. C* **2008**, *112*, 14236−14240.
(50) Sevilla, M.; Fuertes, A. B. Chemical and structural properties of carbonaceous products obtained by hydrothermal carbonization of saccharides. *Chem. - Eur. J.* **2009**, *15*, 4195−4203.
(51) Nizamuddin, S.; Baloch, H. A.; Griffin, G. J.; Mubarak, N. M.; Bhutto, A. W.; Abro, R.; Mazari, S. A.; Ali, B. S. An overview of effect of process parameters on hydrothermal carbonization of biomass. *Renewable Sustainable Energy Rev.* **2017**, *73*, 1289−1299.
(52) Li, R.; Wang, L.; Shahbazi, A. A review of hydrothermal carbonization of carbohydrates for carbon spheres preparation. *Trends Renew. Energy* **2015**, *1*, 43−56.
(53) Song, Y.; Zhu, S.; Zhang, S.; Fu, Y.; Wang, L.; Zhao, X.; Yang, B. Investigation from chemical structure to photoluminescent mechanism: a type of carbon dots from the pyrolysis of citric acid and an amine. *J. Mater. Chem. C* **2015**, *3*, 5976−5984.
(54) Sahu, S.; Behera, B.; Maiti, T. K.; Mohapatra, S. Simple one-step synthesis of highly luminescent carbon dots from orange juice: application as excellent bio-imaging agents. *Chem. Commun.* **2012**, *48*, 8835−8837.

DOI: 10.1021/acs.langmuir.9b00920
Langmuir 2019, 35, 6708−6718

(55) Lee, W. H.; Lee, J. G.; Reucroft, P. J. XPS study of carbon fiber surfaces treated by thermal oxidation in a gas mixture of $O_2/(O_2+N_2)$. *Appl. Surf. Sci.* **2001**, *171*, 136−142.
(56) López, G. P.; Castner, D. G.; Ratner, B. D. XPS O 1s binding energies for polymers containing hydroxyl, ether, ketone and ester groups. *Surf. Interface Anal.* **1991**, *17*, 267−272.
(57) Khan, S.; Gupta, A.; Verma, N. C.; Nandi, C. K. Time-resolved emission reveals ensemble of emissive states as the origin of multicolor fluorescence in carbon dots. *Nano Lett.* **2015**, *15*, 8300−8305.
(58) Zhou, Y.; Mintz, K.; Oztan, C.; Hettiarachchi, S.; Peng, Z.; Seven, E.; Liyanage, P.; De La Torre, S.; Celik, E.; Leblanc, R. Embedding carbon dots in superabsorbent polymers for additive manufacturing. *Polymers* **2018**, *10*, 921−932.
(59) Hsu, P.-C.; Chang, H.-T. Synthesis of high-quality carbon nanodots from hydrophilic compounds: role of functional groups. *Chem. Commun.* **2012**, *48*, 3984−3986.
(60) You, S. S.; Rashkov, R.; Kanjanaboos, P.; Calderon, I.; Meron, M.; Jaeger, H. M.; Lin, B. Comparison of the mechanical properties of self-assembled langmuir monolayers of nanoparticles and phospholipids. *Langmuir* **2013**, *29*, 11751−11757.
(61) Liu, W.; Li, S.; Wang, Z.; Yan, E. C. Y.; Leblanc, R. M. Characterization of Surface-Active Biofilm Protein BslA in Self-Assembling Langmuir Monolayer at the Air-Water Interface. *Langmuir* **2017**, *33*, 7548−7555.

DOI: 10.1021/acs.langmuir.9b00920
Langmuir 2019, 35, 6708−6718